Supplementary Information:

Prediction of NMR Parameters and geometry in ^{133}Cs-containing compounds using Density Functional Theory

N. Manukovsky[1], N. Vaisleib[1], M. Arbel-Haddad[2], A. Goldbourt[1]

[1]School of Chemistry, Tel Aviv University, Ramat Aviv 6997801, Tel Aviv, Israel
[2]Nuclear Research Center Negev, PO Box 9001, Beer Sheva 84901, Israel

Computational parameters

Table S1 lists the energy cutoff values and Monkhorst-Pack grid dimensions used in each calculation.

Table S1: energy cutoff and grid sizes used for the calculations.

system	Ecut [Ry]	kgrid xyz
CsF	100	12 12 12
CsCl	80	8 8 8
CsBr	100	8 8 8
CsI	100	8 8 8
Cs_2CrO_4	80	5 6 4
$CsClO_4$	100	7 6 4
Cs_2SO_4	100	8 6 5
$CsVO_3$	110	10 7 10
$CsGeCl_3$	100	12 12 12
$CsGeBr_3$	100	12 12 12
$CsGeI_3$	100	12 12 12
$CsCd(SCN)_3$	70	4 6 3
$CsBPh_4$	70	4 4 4
$[Cs^+(C222)]I^-$	90	3 3 3
CsB_3O_5	90	5 4 3
$CsSc_3F_{10}$	90	5 5 6
$CsPbI_3$, hexagonal	110	4 8 2
$CsPbI_3$, tetragonal	110	5 5 3

Crystal structures and unit cell volumes

Table S2 specifies the experimental and computational unit cell volumes, as well as the references for the crystal structures used as input for the structural optimizations.

Table S2: Experimental and calculated unit cell volumes [Å^3] of the tested materials

	Exp	ref	PBE	rVV10	vdW-DF3-opt1	vdW-DF-C6	rev-vdW-DF2	PBE+ XDM	PBE+ D3	PBE + D2 Zhang	rPBE+ D2 Zhang	rPBE+ D2*	rPBE+ D2* Zhang	revPBE+ D3	PBEsol+ D2 Zhang	PBEsol+ D3	B86bPBE+ XDM
CsF	54.22	[1]	57.11	53.52	52.02	53.56	54.12	41.56	56.28	51.87	56.55	36.03	55.24	61.19	48.10	51.99	47.30
CsCl	70.09	[2]	74.24	68.54	66.25	68.22	68.92	50.97	74.36	67.51	72.80	48.64	72.80	79.42	63.21	67.32	58.74
CsBr	78.73	[2]	83.87	78.02	78.24	78.75	78.68	57.86	84.48	75.92	78.73	55.50	81.50	90.59	70.99	75.97	66.37
CsI	95.24	[2]	101.49	93.22	90.17	92.81	93.87	68.7 2	102.04	89.09	95.27	68.18	95.27	111.48	83.86	90.65	79.61
Cs_2CrO_4	594.61	[3]	630.09	587.09	572.47	585.99	591.49	492.05	620.04	574.66	618.24	463.99	616.76	658.95	536.45	573.54	546.63
$CsClO_4$	458.28	[4]	499.01	447.12	438.86	449.31	455.34	401.77	480.19	455.49	497.34	417.34	497.02	499.35	425.70	450.57	429.84
Cs_2SO_4	563.72	[5]	602.80	559.22	544.48	556.51	561.45	475.88	592.37	555.57	594.91	444.64	586.52	625.40	522.00	549.93	475.88
$CsVO_3$	382.21	[6]	418.31	381.22	371.36	380.15	384.94	356.19	408.41	374.63	409.59	335.44	408.01	427.01	349.24	375.67	354.54
$CsGeCl_3$	161.43	[7]	169.12	152.18	145.96	150.68	152.20	133.52	163.34	147.76	171.30	145.74	171.76	167.85	134.47	146.70	140.68
$CsGeBr_3$	179.98	[7]	189.43	174.38	165.74	170.85	173.06	153.34	181.75	165.04	185.94	160.81	186.76	185.40	153.50	164.10	159.23
$CsGeI_3$	215.37	[7]	228.01	214.47	203.09	208.46	211.53	184.93	219.52	199.25	218.47	193.80	216.10	227.74	185.48	200.71	194.96
$CsCd(SCN)_3$	967.6	[8]	1077.6	946.4		938.9	951.3		1010.1					1038.0		927.0	
$CsBPh_4$	536.4	[9]	609.7	502.2		500.9	510.7		545.1					602.7		503.0	
$[Cs^+(C222)]I^-$	1235.4	[10]	1438.2	1174.8		1183.6	1208.8		1234.5					1215.7		1144.4	
CsB_3O_5	480.6	[11]	522.7	488.6		484.7	489.2		505.4					516.9		480.0	
$CsSc_3F_{10}$	417.2	[12]	433.8	416.9		421.5	423.2		430.6					440.7		413.6	
$CsPbI_3$, hexagonal	892.7	[14]	964.0	895.0		883.9	897.5		934.3					975.9		855.1	
$CsPbI_3$, tetragonal	947.3	[15]	1005.3	939.5		929.9	947.5		983.8					1011.9		913.5	

Additional error metrics

Figure S1 shows additional statistical parameters of the DFT calculations.

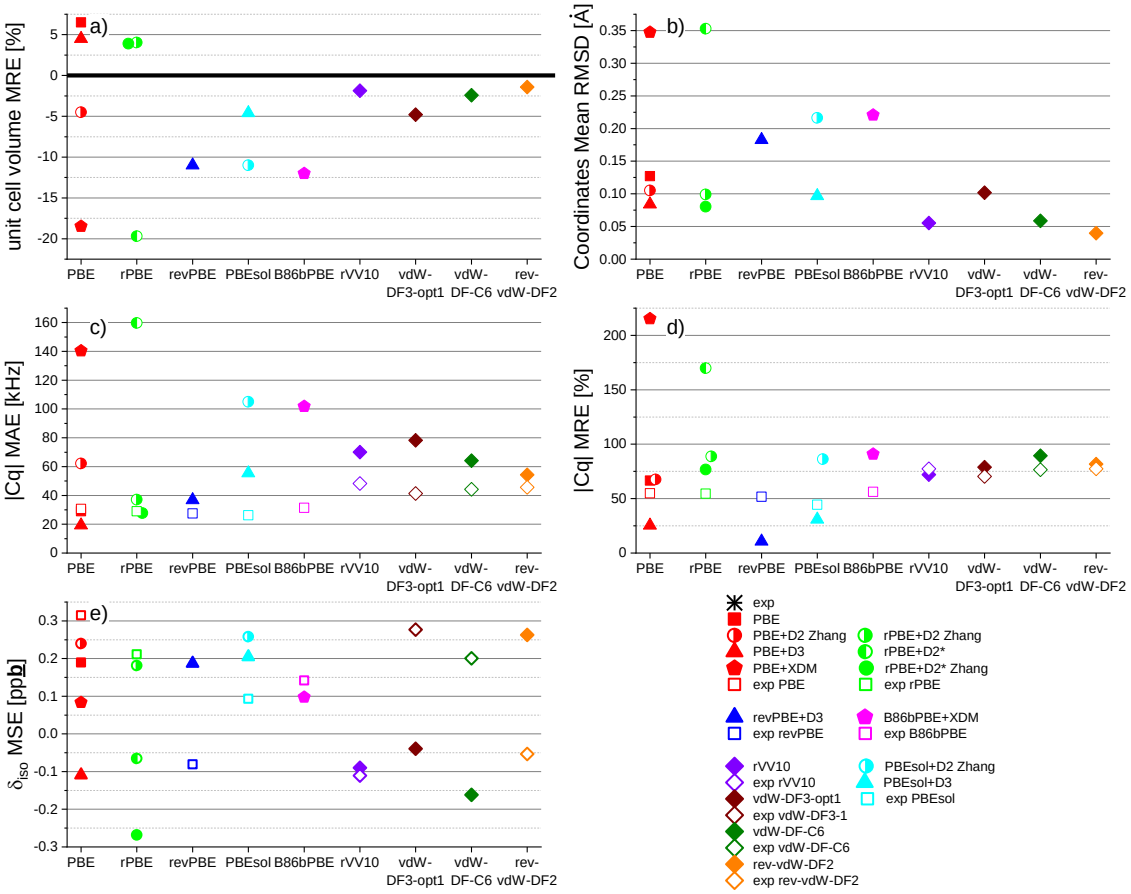

Figure S1: Error metrics of DFT functionals: a) Mean Relative Error of the unit cell volume; b) Mean RMSD of the atom coordinates; c) Mean Absolute Error and d) Mean Relative Error of the quadrupolar coupling constant; e) Mean Signed Error of the isotropic chemical shift, in ppb.

Quadrupolar coupling constants

Table S3 – Table S6 specify the experimental and computational quadrupolar coupling parameters of the tested materials.

Table S3: Experimental quadrupolar coupling constants of the tested materials

	Experimental		
	|Cq| [kHz]	**η**	**ref**
CsF	0	0	
CsCl	0	0	
CsBr	0	0	
CsI	0	0	
Cs_2CrO_4 I	365	0.56	[16]
	376	0.52	[17]
	373	0.55	[18]
Cs_2CrO_4 II	142	0.11	[16]
	138	0.15	[17]
	142	0.15	[18]
$CsClO_4$	133.6	0.11	[16]
Cs_2SO_4 I	20	0.27	[16]
Cs_2SO_4 II	261	0.01	[16]
$CsVO_3$	225	0.47	[16]
$CsGeCl_3$	12	<0.10	[7]
$CsGeBr_3$	52 50	0 0	[7]
$CsGeI_3$	55 52	0.05 0.05	[7]
$CsCd(SCN)_3$	148	0.98	[19]
$CsBPh_4$	335	NA	[20]
[Cs^+(Cryptand[2.2.2])]I^-	1047	0.73	[10]
CsB_3O_5	380	NA	[21]
$CsSc_3F_{10}$	NA	NA	
$CsPbI_3$, hexagonal	NA	NA	
$CsPbI_3$, tetragonal	NA	NA	

Table S4: Calculated quadrupolar coupling constants – PBE and rPBE functionals

	PBE		Exp PBE		PBE + D2 Zhang		PBE+D3		PBE+XDM		rPBE + D2 Zhang		rPBE +D2*		rPBE +D2* Zhang		exp rPBE	
	Cq [kHz]	η	Cq [kHz]	η	Cq [kHz]	η	Cq [kHz]	η	Cq [kHz]	η	Cq [kHz]	η	Cq [kHz]	η	Cq [kHz]	η	Cq [kHz]	η
Cs_2CrO_4 I	391	0.6	456	0.6	487	0.4	396	0.6	725	0.4	373	0.6	544	0.8	393	0.6	445	0.5
Cs_2CrO_4 II	-136	0.5	-152	0.2	-183	0.4	-142	0.0	-193	0.1	-154	0.3	-450	0.0	-141	0.3	-153	0.3
$CsClO_4$	156	0.3	194	0.8	304	0.1	203	0.2	430	0.2	218	0.3	406	0.1	155	0.3	189	0.8
Cs_2SO_4 I	278	0.3	289	0.0	293	0.2	269	0.1	359	0.2	275	0.2	342	0.2	274	0.3	281	0.0
Cs_2SO_4 II	82	0.3	64	0.6	116	0.5	43	0.1	242	0.2	79	0.5	212	0.6	84	0.3	62	0.7
$CsVO_3$	140	0.2	238	0.3	266	0.3	195	0.8	373	0.8	146	0.5	571	1.0	159	0.5	244	0.1
$CsGeCl_3$	41	0.0	28	0.0	11	0.0	20	0.0	53	0.0	56	0.0	8	0.0	48	0.0	29	0.0
$CsGeBr_3$	60	0.0	56	0.0	20	0.0	43	0.0	17	0.0	73	0.0	17	0.0	64	0.0	57	0.0
$CsGeI_3$	66	0.0	66	0.0	25	0.0	54	0.0	70	0.0	69	0.0	29	0.0	67	0.0	68	0.0
$CsCd(SCN)_3$	217	0.6					160	1.0										
$CsBPh_4$	258	0.0					275	0.0										
$[Cs^+(C222)]I^-$	959	0.7					982	0.9										
CsB_3O_5	-465	0.7					-436	0.5										
$CsSc_3F_{10}$	-431	0.8					-432	0.8										

Table S5: Calculated quadrupolar coupling constants – additional semilocal functionals

	revPBE + D3		exp revPBE		PBEsol + D2 Zhang		PBEsol + D3		exp PBEsol		B86bPBE + XDM		exp B86bPBE	
	Cq [kHz]	η	Cq [kHz]	η	Cq [kHz]	η	Cq [kHz]	η	Cq [kHz]	η	Cq [kHz]	η	Cq [kHz]	η
Cs_2CrO_4 I	276	0.8	444	0.5	616	0.3	506	0.6	451	0.6	573	0.6	458	0.6
Cs_2CrO_4 II	-136	0.6	-153	0.3	-184	0.4	-155	0.0	-150	0.1	-169	0.1	-153	0.2
$CsClO_4$	223	0.1	189	0.8	366	0.0	242	0.3	189	0.7	326	0.3	195	0.8
Cs_2SO_4 I	258	0.0	282	0.0	327	0.1	290	0.0	291	0.0	323	0.2	290	0.0
Cs_2SO_4 II	30	0.3	62	0.7	148	0.3	75	0.5	58	0.7	157	0.2	66	0.6
$CsVO_3$	116	0.8	237	0.2	350	0.2	310	0.8	221	0.5	425	0.4	239	0.3
$CsGeCl_3$	20	0.0	27	0.0	3	0.0	3	0.0	25	0.0	3	0.0	28	0.0
$CsGeBr_3$	41	0.0	55	0.0	3	0.0	15	0.0	50	0.0	0	0.0	56	0.0
$CsGeI_3$	57	0.0	65	0.0	6	0.0	28	0.0	59	0.0	18	0.0	66	0.0
$CsCd(SCN)_3$	133	0.9					210	0.6						
$CsBPh_4$	215	0.0					296	0.0						
$[Cs^+(Cryptand[2.2.2])]I^-$	952	0.9					1020	0.9						
CsB_3O_5	-335	0.7					-499	0.7						
$CsSc_3F_{10}$	-386	0.9					-469	0.7						

Table S6: Calculated quadrupolar coupling constants – nonlocal functionals

	rVV10		exp rVV10		vdW-DF3-opt1		exp vdW-DF3-opt1		vdW-DF-C6		exp vdW-DF-C6		rev-vdW-DF2		exp rev-vdW-DF2	
	Cq [kHz]	**η**	**Cq [kHz]**	**η**	**Cq [kHz]**	**η**	**Cq [kHz]**	**η**	**Cq [kHz]**	**η**	**Cq [kHz]**	**η**	**Cq [kHz]**	**η**	**Cq [kHz]**	**η**
Cs_2CrO_4 I	529	0.6	500	0.6	539	0.6	479	0.6	511	0.6	488	0.6	496	0.6	486	0.6
Cs_2CrO_4 II	-158	0.2	-154	0.3	-158	0.3	-153	0.3	-155	0.3	-154	0.3	-152	0.3	-154	0.3
$CsClO_4$	300	0.2	218	0.7	310	0.3	210	0.8	289	0.2	194	0.8	259	0.3	214	0.8
Cs_2SO_4 I	319	0.2	309	0.1	322	0.2	301	0.1	315	0.2	303	0.1	310	0.2	302	0.1
Cs_2SO_4 II	104	0.4	82	0.5	120	0.5	76	0.6	105	0.5	80	0.6	99	0.5	80	0.6
$CsVO_3$	354	0.5	272	0.2	358	0.5	257	0.3	323	0.5	270	0.2	296	0.4	268	0.2
$CsGeCl_3$	8	0.0	31	0.0	12	0.0	31	0.0	28	0.0	33	0.0	28	0.0	33	0.0
$CsGeBr_3$	37	0.0	63	0.0	27	0.0	61	0.0	41	0.0	65	0.0	44	0.0	65	0.0
$CsGeI_3$	54	0.0	73	0.0	29	0.0	72	0.0	58	0.0	77	0.0	61	0.0	77	0.0
$CsCd(SCN)_3$	-244	0.6							-255	0.6			-245	0.7		
$CsBPh_4$	327	0.0							344	0.0			347	0.0		
$[Cs^+(Cryptand[2.2.2])]I^-$	1069	0.9							1072	1.0			1071	0.9		
CsB_3O_5	-541	0.5							-494	0.8			-485	0.7		
$CsSc_3F_{10}$	-555	0.9							-519	0.6			-515	0.6		

Scaling the quadrupolar coupling constants

Figure S2 and Table S7 show a fairly linear, though noisy, correlation between the computational |Cq| obtained by various functionals (shown are the best performing functionals in terms of Cq). Similar trends were reported for ^{133}Cs[22] and for several other half-integer quadrupolar nuclei[23].

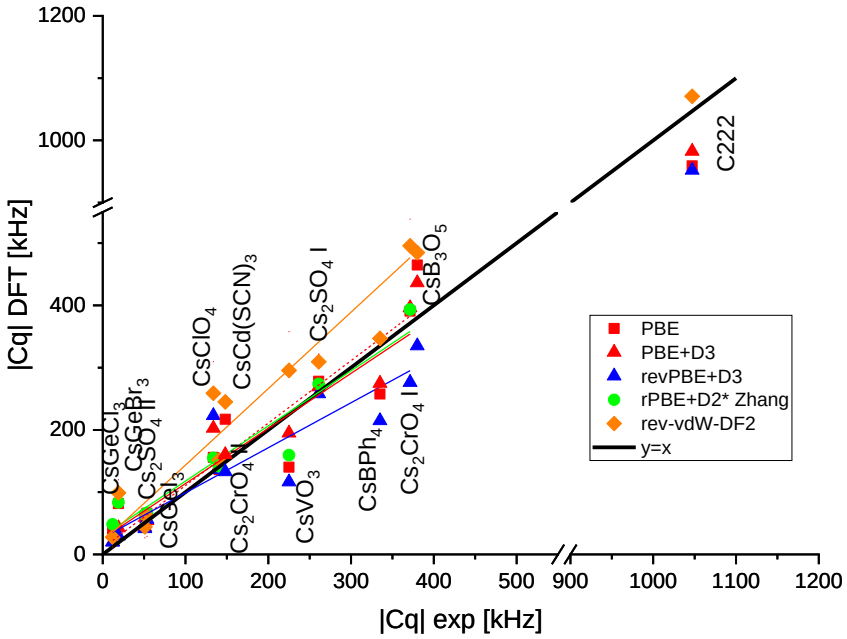

Figure S2: Calculated vs experimental quadrupolar coupling constants of selected functionals.

Table S7: linear fit parameters for Figure S2.

functional	Intercept±SE [kHz]	Slope±SE	R^2
PBE	31 ± 19	0.89 ± 0.05	0.98
PBE+D3	20 ± 13	0.93 ± 0.04	0.99
revPBE+D3	1 ± 19	0.87 ± 0.05	0.98
PBEsol+D3	40 ± 25	0.99 ± 0.07	0.97
rVV10	63 ± 27	1.01 ± 0.08	0.97
rev-vdW-DF2	54 ± 19	1.00 ± 0.05	0.99
vdW-DF-c6	62 ± 22	1.00 ± 0.06	0.98
rPBE+D2* Zhang	29 ± 18	0.89 ± 0.10	0.96

^{87}Rb Quadrupolar coupling constants

The quadrupolar coupling constant of ^{133}Cs is small due its low quadrupolar moment (-0.00343 b[24]). This raised the question whether the differences between Cq values obtained by various functionals fall within the error range. To check this, we performed similar calculations using a nucleus with a much larger quadrupolar moment (0.1335 b[24]) – ^{87}Rb. The results (Figure S3) show the same trend observed in ^{133}Cs repeats itself in ^{87}Rb. We therefore conclude that the differences between Cq of various functionals reflect inherent differences between these functionals.

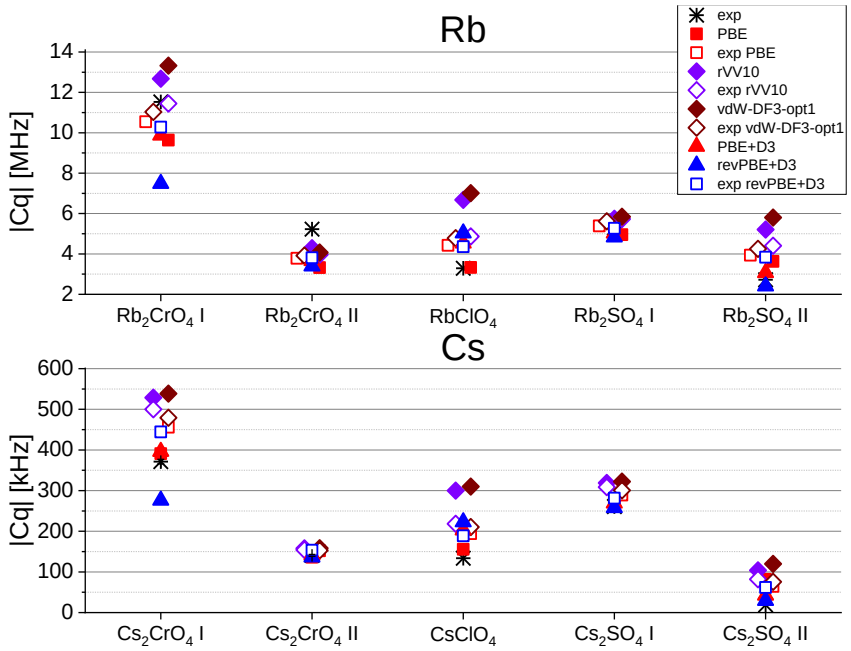

Figure S3: Quadrupolar coupling constants of Rb salts, compared with Cs salts. The experimental ^{87}Rb data are taken from previously reported studies[25–27].

Chemical Shifts

Table S8 – S12 specify the experimental and computational ^{133}Cs chemical shift parameters of the materials discussed in the main text.

To generate consistent experimental values, we re-referenced the results of several studies to fit a uniform scale, where solid CsCl resonates at 223.2 ppm, as commonly used in solid-state NMR studies. Since some studies also used 0.5M or 1.0M solutions of CsCl as a reference[28] and some studies were performed at static conditions, we also acquired our own data at room temperature using a 14.1T magnet and 5 kHz spinning. We measured solid samples of CsCl, CsI, Cs_2CrO_4, and Cs_2SO_4. We also performed experiments on 5 solutions of CsCl at different concentrations at the range of 0.1-1.0 [M] and obtained a linear fit where $\delta_{iso}(^{133}\mathrm{Cs, ppm}) = 11.3(0.2)\left[\frac{\mathrm{M}}{\mathrm{ppm}}\right] - 6.1(0.2)[\mathrm{ppm}]$. This result was obtained by referencing all data to solid CsCl at 223.2 ppm and is consistent with infinite dilution values reported by Haase[29] though with some deviations for his reported value of 0.5M CsCl.

Our experimental results are shown in the top of Figure S4. To demonstrate the relation between solid CsCl and a 0.1M solution of $CsNO_3$ in D_2O, as recommended by IUPAC, we measured the two samples at static conditions and at two temperatures (bottom of Figure S4). While the solid sample is not affected by the temperature, the solution shows a shift of 1.9 ppm over 15°C, suggesting a strong temperature dependence.

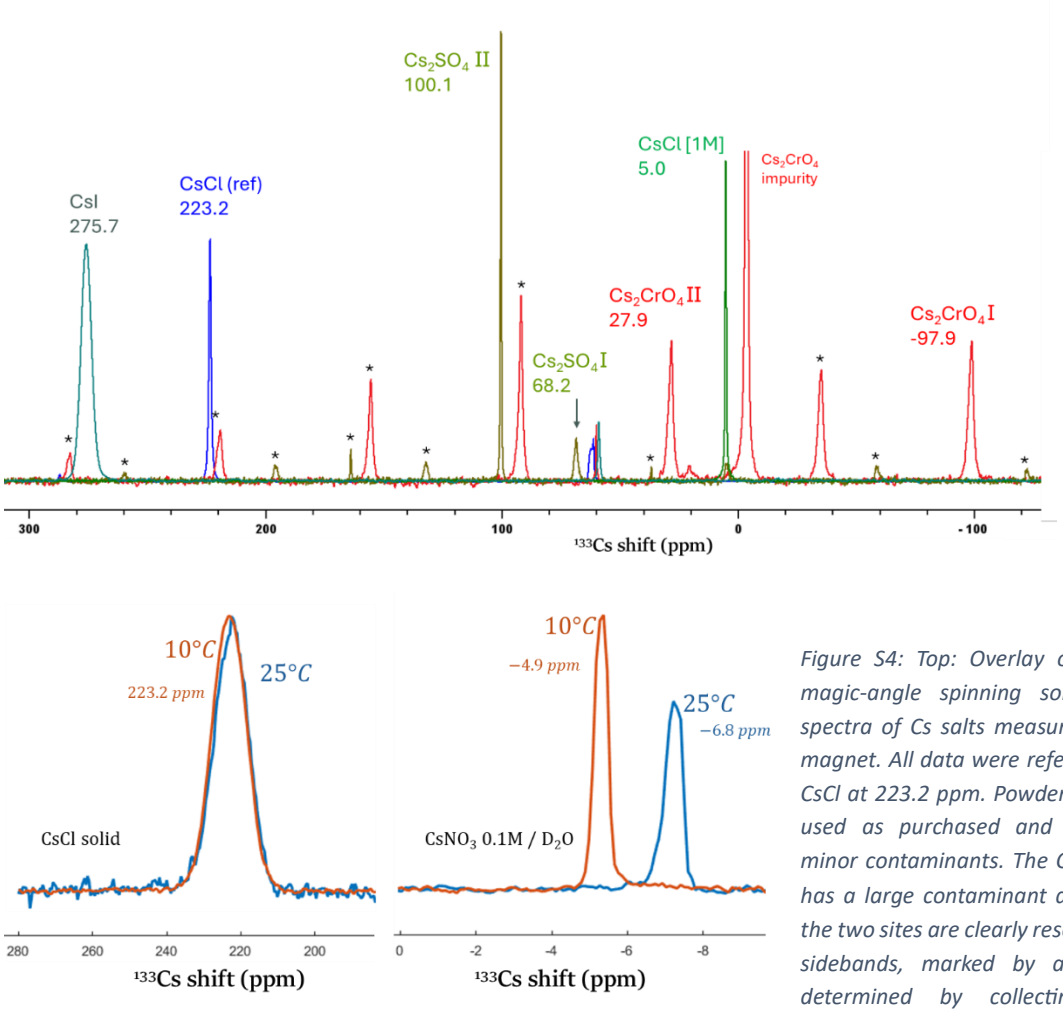

Figure S4: Top: Overlay of ^{133}Cs 5 kHz magic-angle spinning solid-state NMR spectra of Cs salts measured on a 14.1T magnet. All data were referenced to solid CsCl at 223.2 ppm. Powder samples were used as purchased and contain some minor contaminants. The Cs_2CrO_4 sample has a large contaminant at ~0 ppm but the two sites are clearly resolved. Spinning sidebands, marked by asterisks, were determined by collecting additional experiments at 6.66 and 7.50 kHz. Bottom: Static spectra of powdered CsCl (left) and a 0.1M solution of $CsNO_3$ in D_2O (right, IUPAC recommendation) at 10°C and 25°C. The powder of $CsNO_3$ was initially dried in the oven since it is highly hygroscopic.

Table S8: Experimental chemical shifts [ppm] of the materials examined in this work.

Experimental				
	δ_{iso}	$\Delta\delta = \delta_{zz}-(\delta_{xx}+\delta_{yy})/2$	$\eta=(\delta_{yy}-\delta_{xx})/(\delta_{zz}-\delta_{iso})$	ref
CsF	181.3*	0	0	[28]
CsCl	223.2	0	0	[30]
CsBr	256.0*	0	0	[28]
	258.2	0	0	[30]
CsI	276.1*	0	0	[28]
	275.7	0	0	This work
Cs_2CrO_4 I	-98.3^	-328.5	0.04	[18]
	-98.3	-331.5	0.06	[16]
	-100	-333	0.04	[17]
	-97.9			This work
Cs_2CrO_4 II	28.7^	246	0.3	[18]
	28.2	243	0.31	[16]
	27.0	244.5	0.26	[17]
	27.9			This work
$CsClO_4$	2.7	34.35	0.32	[16]
Cs_2SO_4 I	68.6	-22.45	0.14	[16]
	68.2			This work
Cs_2SO_4 II	100.3	-46.5	0.49	[16]
	100.1			This work
$CsVO_3$	-32.0	-135	0.44	[16]
$CsGeCl_3$	36.9 33.7	10 10	0 0	[7]
$CsGeBr_3$	48.2 47.5	-9 16	1 0	[7]
$CsGeI_3$	41.8 39.2	NA	NA	[7]
$CsCd(SCN)_3$	54.7^	83.8	0.38	[19]
$CsBPh_4$	-272*	36.5	0	[20]
$[Cs^+(Cryptand[2.2.2])]I^-$	225	39	0.92	[31]
CsB_3O_5	70.9*	120	NA	[21]
$CsSc_3F_{10}$	-1.8^	NA	NA	[12]
$CsPbI_3$, hexagonal	245*	NA	NA	[32]
$CsPbI_3$, tetragonal	119.1*	NA	NA	[32]

** Originally referenced to 1.0 M CsCl=0 ppm. Our measurements show that with respect to solid CsCl at 223.2 ppm, the shift is +5.0 ppm.*

^ Originally referenced to 0.5 M CsCl=0 ppm. Our measurements show that with respect to solid CsCl at 223.2 ppm, the shift is -0.6 ppm.

Table S9: Calculated Chemical shifts [ppm] – PBE functionals

	PBE			Exp PBE			PBE + D2 Zhang			PBE+D3			PBE+XDM		
	δ_{iso}	Δδ	η	δ_{iso}	Δδ	η	δ_{iso}	Δδ	η	δ_{iso}	Δδ	η	δ_{iso}	Δδ	η
CsF	198.8	0	0	200.2	0	0	196.3	0	0	209.3	0	0	226.3	0	0
CsCl	230.7	0	0	226.5	0	0	216.4	0	0	226.3	0	0	241.6	0	0
CsBr	261.6	0	0	268.3	0	0	251.9	0	0	254.7	0	0	259.1	0	0
CsI	270.5	0	0	276.2	0	0	291.7	0	0	266.0	0	0	273.1	0	0
Cs_2CrO_4 I	-69.4	-277.0	0.16	-69.5	-309.3	0.28	-85.7	-347.0	0.42	-84.7	-276.5	0.03	-41.2	-453.6	0.44
Cs_2CrO_4 II	26.8	356.3	0.01	37.2	378.0	0.02	32.1	389.2	0.07	25.5	350.3	0.03	56.1	541.5	0.05
$CsClO_4$	5.4	43.9	0.38	14.1	50.2	0.90	-0.3	63.1	0.19	15.5	52.9	0.25	7.8	81.1	0.56
Cs_2SO_4 I	74.1	38.1	0.91	69.3	-47.0	0.16	57.3	-46.0	0.48	72.7	-38.5	0.79	59.7	-78.7	0.20
Cs_2SO_4 II	103.8	19.8	0.62	102.5	17.2	0.16	90.2	-10.5	0.58	103.9	-11.3	0.50	96.5	-30.4	0.45
$CsVO_3$	-34.7	-165.9	0.30	-13.6	-172.0	0.46	-19.6	-186.2	0.58	-36.1	-159.7	0.45	-29.1	-190.5	0.28
$CsGeCl_3$	9.8	-19.9	0	-9.6	-16.9	0.00	26.6	-9.4	0.00	12.2	-12.5	0.00	3.2	-9.9	0.00
$CsGeBr_3$	29.8	-24.8	0	13.7	-23.5	0.00	42.0	-11.0	0.00	38.4	-17.5	0.00	-16.5	-22.5	0.00
$CsGeI_3$	18.9	-12.9	0	10.9	-14.9	0.00	27.2	-9.5	0.00	22.5	-9.5	0.00	-10.4	-22.2	0.00
$CsCd(SCN)_3$	10.8	120.8	0.40							32.7	111.4	0.38			
$CsBPh_4$	-223.7	48.5	0.00							-250.8	55.1	0.00			
$[Cs^+(Cryptand[2.2.2])]I^-$	254.3	-22.6	0.92							264.9	-9.7	0.33			
CsB_3O_5	70.2	106.7	0.67							69.5	95.6	0.88			
$CsSc_3F_{10}$	42.8	-116.1	0.41							29.5	-118.2	0.41			
$CsPbI_3$, hexagonal	228.7									265.8					
$CsPbI_3$, tetragonal	184.1									127.2					

Table S10: Calculated Chemical shifts [ppm] – rPBE functionals

	rPBE + D2 Zhang			rPBE +D2*			rPBE +D2* Zhang			exp rPBE		
	δ_{iso}	Δδ	η	δ_{iso}	Δδ	η	δ_{iso}	Δδ	η	δ_{iso}	Δδ	η
CsF	178.3	0.0	0.00	323.8	0.0	0.00	199.0	0.0	0.00	198.8	0.0	0.00
CsCl	210.6	0.0	0.00	234.3	0.0	0.00	210.0	0.0	0.00	221.0	0.0	0.00
CsBr	282.8	0.0	0.00	247.9	0.0	0.00	277.4	0.0	0.00	268.5	0.0	0.00
CsI	291.6	0.0	0.00	238.5	0.0	0.00	280.4	0.0	0.00	275.4	0.0	0.00
Cs_2CrO_4 I	-60.0	-273.1	0.31	-21.8	-553.1	0.36	-58.8	-262.4	0.23	-80.6	-281.6	0.27
Cs_2CrO_4 II	38.4	313.6	0.06	91.5	331.9	0.35	30.5	331.6	0.01	22.2	351.5	0.01
$CsClO_4$	0.6	48.3	0.12	-29.5	71.2	0.40	-7.4	40.7	0.42	13.2	50.2	0.90
Cs_2SO_4 I	69.2	33.8	0.89	88.1	-81.3	0.23	74.7	-37.2	0.81	78.8	-42.4	0.24
Cs_2SO_4 II	93.4	8.4	0.88	99.8	-60.7	0.97	102.1	16.7	0.56	110.2	14.8	0.30
$CsVO_3$	-20.6	-151.5	0.41	-13.4	209.1	0.99	-22.6	-152.6	0.34	2.1	-158.8	0.47
$CsGeCl_3$	-11.0	-21.4	0.00	-49.8	-12.0	0.00	-14.4	-19.6	0.00	-10.6	-15.2	0.00
$CsGeBr_3$	22.5	-25.3	0.00	-38.8	-13.6	0.00	18.8	-24.9	0.00	14.0	-22.8	0.00
$CsGeI_3$	30.3	-10.0	0.00	-44.4	-17.5	0.00	36.5	-14.6	0.00	13.2	-15.7	0.00

Table S11: Calculated Chemical shifts [ppm] – additional semilocal functionals

	revPBE + D3			exp revPBE			PBEsol + D2 Zhang			PBEsol + D3			exp PBEsol			B86bPBE + XDM			exp B86bPBE		
	δ_{iso}	Δδ	η	δ_{iso}	Δδ	η	δ_{iso}	Δδ	η	δ_{iso}	Δδ	η	δ_{iso}	Δδ	η	δ_{iso}	Δδ	η	δ_{iso}	Δδ	η
CsF	195.1	0.0	0.00	196.9	0.0	0.00	220.1	0.0	0.00	201.1	0.0	0.00	201.7	0.0	0.00	198.3	0.0	0.00	200.1	0.0	0.00
CsCl	235.9	0.0	0.00	230.6	0.0	0.00	217.3	0.0	0.00	223.9	0.0	0.00	238.5	0.0	0.00	238.0	0.0	0.00	224.9	0.0	0.00
CsBr	261.8	0.0	0.00	268.6	0.0	0.00	250.9	0.0	0.00	254.5	0.0	0.00	262.7	0.0	0.00	265.5	0.0	0.00	268.3	0.0	0.00
CsI	250.0	0.0	0.00	277.3	0.0	0.00	279.9	0.0	0.00	275.6	0.0	0.00	270.3	0.0	0.00	278.0	0.0	0.00	275.1	0.0	0.00
Cs_2CrO_4 I	-101.7	-219.6	0.16	-69.5	-288.2	0.26	-88.6	-420.8	0.46	-85.9	-353.7	0.28	-66.0	-321.8	0.31	-69.1	-368.7	0.32	-80.0	-305.4	0.26
Cs_2CrO_4 II	19.8	265.8	0.08	34.4	352.6	0.00	37.7	479.2	0.07	24.7	436.6	0.03	37.5	406.3	0.04	27.6	446.4	0.04	26.2	378.9	0.00
$CsClO_4$	14.6	47.3	0.05	13.6	47.7	0.89	-1.8	73.4	0.48	0.9	62.6	0.50	8.6	51.5	0.99	8.9	72.9	0.43	26.3	50.2	0.90
Cs_2SO_4 I	74.6	32.5	0.67	72.0	-43.0	0.23	52.2	-64.6	0.06	61.0	-54.2	0.11	71.4	-50.9	0.10	55.8	-78.7	0.20	73.1	-47.0	0.16
Cs_2SO_4 II	101.1	-5.2	0.77	104.2	15.1	0.32	92.3	-13.3	0.85	97.0	-14.1	0.86	103.9	18.8	0.04	91.1	-30.4	0.45	106.2	17.2	0.16
$CsVO_3$	-36.1	-128.1	0.52	-1.7	-158.5	0.46	-12.0	-214.8	0.70	-28.1	-195.4	0.59	-18.3	-183.9	0.50	-3.0	-189.1	0.65	-0.8	-168.9	0.44
$CsGeCl_3$	21.4	-11.3	0.00	-12.0	-16.4	0.00	46.0	-8.5	0.00	33.4	-8.4	0.00	-5.6	-17.6	0.00	18.0	-5.8	0.00	-12.3	-16.0	0.00
$CsGeBr_3$	61.6	-16.1	0.00	11.3	-23.2	0.00	6.3	-21.1	0.00	46.9	-13.0	0.00	15.5	-24.7	0.00	16.9	-10.9	0.00	15.0	-23.4	0.00
$CsGeI_3$	28.1	-10.8	0.00	0.4	-14.5	0.00	25.8	-19.9	0.00	21.3	-11.1	0.00	6.1	-14.0	0.00	0.2	-12.7	0.00	4.1	-13.7	0.00
$CsCd(SCN)_3$	38.3	84.6	0.62							47.3	137.5	0.46									
$CsBPh_4$	-320.8	-3.6	0.00							-233.6	74.0	0.00									
$[Cs^+(C222)]I^-$	349.6	20.0	0.39							204.3	16.6	0.42									
CsB_3O_5	57.9	74.0	0.92							52.8	113.6	0.90									
$CsSc_3F_{10}$	48.5	-99.8	0.41							-4.1	-140.7	0.44									
$CsPbI_3$, hexagonal	283.6									272.4											
$CsPbI_3$, tetragonal	-37.7									130.0											

Table S12: Calculated Chemical shifts [ppm] – non-local functionals

	rVV10			exp rVV10			vdW-DF3-opt1			exp vdW-DF3-opt1			vdW-DF-C6			exp vdW-DF-C6			rev-vdW-DF2			exp rev-vdW-DF2		
	δ_{iso}	Δδ	η	δ_{iso}	Δδ	η	δ_{iso}	Δδ	η	δ_{iso}	Δδ	η	δ_{iso}	Δδ	η	δ_{iso}	Δδ	η	δ_{iso}	Δδ	η	δ_{iso}	Δδ	η
CsF	190.5	0.0	0.00	194.6	0.0	0.00	196.6	0.0	0.00	191.1	0.0	0.00	188.9	0.0	0.00	210.6	0.0	0.00	185.8	0.0	0.00	193.4	0.0	0.00
CsCl	223.6	0.0	0.00	227.4	0.0	0.00	240.0	0.0	0.00	226.2	0.0	0.00	233.1	0.0	0.00	242.8	0.0	0.00	231.4	0.0	0.00	223.9	0.0	0.00
CsBr	254.5	0.0	0.00	266.0	0.0	0.00	226.2	0.0	0.00	267.6	0.0	0.00	241.2	0.0	0.00	281.2	0.0	0.00	251.7	0.0	0.00	263.4	0.0	0.00
CsI	279.2	0.0	0.00	276.0	0.0	0.00	283.4	0.0	0.00	273.2	0.0	0.00	280.5	0.0	0.00	224.0	0.0	0.00	275.4	0.0	0.00	273.2	0.0	0.00
Cs_2CrO_4 I	-99.4	-352.5	0.30	-74.1	-341.5	0.30	-101.8	-359.9	0.30	-83.8	-325.5	0.30	-100.4	-339.2	0.30	-84.5	-327.0	0.30	-95.7	-331.7	0.30	-86.9	-325.8	0.30
Cs_2CrO_4 II	21.9	433.4	0.00	37.9	426.4	0.00	19.3	441.2	0.00	26.6	410.0	0.00	19.1	419.1	0.00	34.9	405.7	0.00	19.6	411.9	0.00	22.1	404.6	0.00
$CsClO_4$	39.1	74.2	0.23	14.7	54.7	0.87	30.4	71.5	0.36	17.8	52.1	0.87	29.8	68.6	0.23	-0.2	50.2	0.90	25.9	64.4	0.29	26.4	53.0	0.84
Cs_2SO_4 I	68.9	-51.2	0.38	64.3	-54.6	0.04	68.6	-54.8	0.21	77.4	-51.4	0.09	70.6	-51.0	0.28	83.6	-52.2	0.04	71.9	-49.4	0.32	74.1	-51.6	0.04
Cs_2SO_4 II	107.3	-18.3	0.52	98.5	21.0	0.09	111.0	-18.0	0.87	112.0	19.8	0.09	110.0	-16.0	0.95	120.4	19.7	0.10	109.3	-15.3	1.00	107.8	19.6	0.07
$CsVO_3$	-21.1	-189.9	0.51	-25.4	-192.5	0.45	-26.1	-193.6	0.58	-5.4	-179.1	0.43	-25.3	-183.8	0.51	-26.0	-181.7	0.47	-28.2	-181.8	0.51	-21.8	-182.5	0.49
$CsGeCl_3$	28.0	-7.2	0.00	-2.5	-17.3	0.00	35.0	-9.5	0.00	-3.9	-17.5	0.00	30.0	-13.1	0.00	-3.3	-16.6	0.00	32.2	-13.2	0.00	6.2	-18.3	0.00
$CsGeBr_3$	29.9	-11.9	0.00	27.3	-24.2	0.00	36.9	-12.7	0.00	18.3	-24.2	0.00	36.1	-12.4	0.00	26.1	-23.8	0.00	35.4	-14.0	0.00	26.7	-23.9	0.00
$CsGeI_3$	3.8	-3.3	0.00	21.6	-11.8	0.00	6.6	-8.5	0.00	8.9	-12.9	0.00	12.4	-6.3	0.00	16.6	-12.4	0.00	11.5	-6.6	0.00	17.5	-12.5	0.00
$CsCd(SCN)_3$	66.4	137.4	0.85										68.6	138.0	0.39				63.7	136.3	0.39			
$CsBPh_4$	-252.5	67.8	0.00										-244.1	73.7	0.00				-237.3	73.0	0.00			
$[Cs^+(C222)]I^-$	198.7	30.4	0.04										223.6	22.7	0.09				228.7	19.2	0.11			
CsB_3O_5	77.7	118.1	0.96										71.7	118.0	0.84				69.5	110.5	0.81			
$CsSc_3F_{10}$	12.8	-122.9	0.05										-9.1	-129.8	0.38				-1.6	-130.4	0.41			
$CsPbI_3$, hexagonal	274.0												271.7						257.6					
$CsPbI_3$, tetragonal	238.7												221.7						219.8					

Chemical Shift Anisotropy

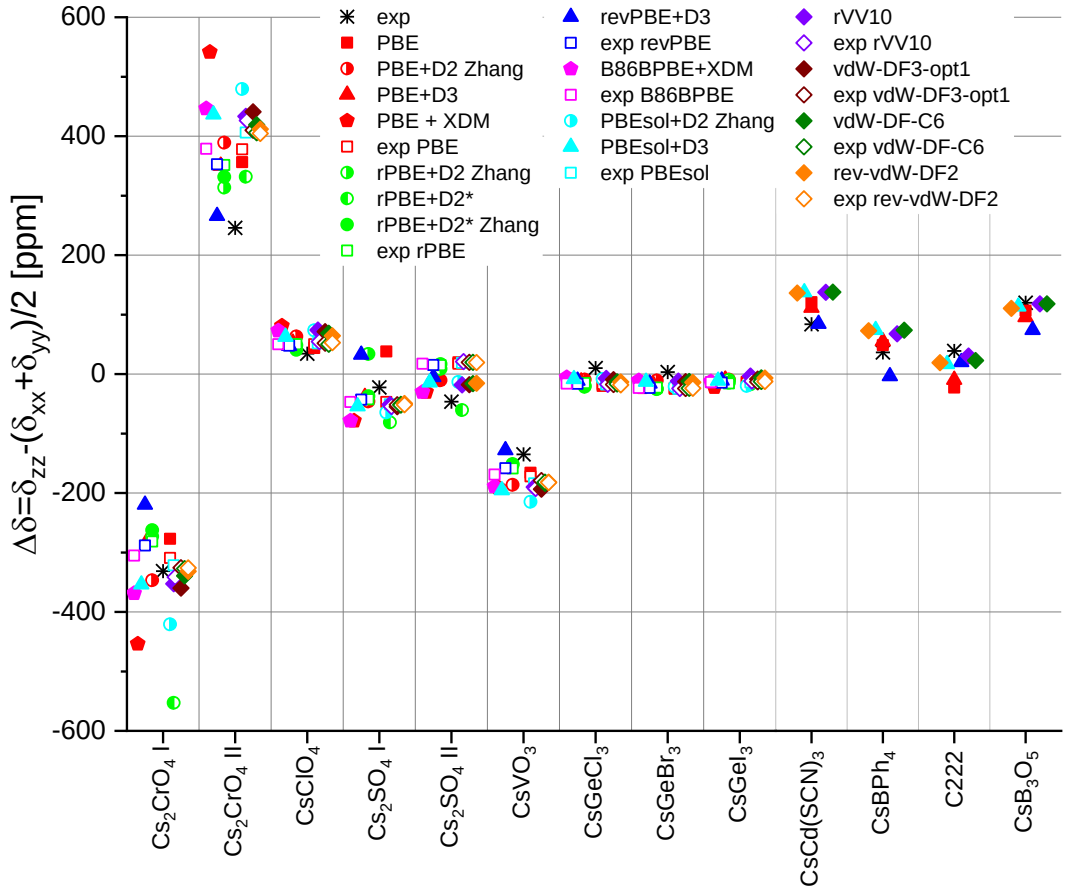

Figure S5: Calculated vs experimental chemical shift anisotropies.

Fully relativistic geometry optimization

The calculations in this work were performed using scalar-relativistic pseudopotentials, as GIPAW currently does not support non-collinear calculations and geometry calculations require heavy computational resources. In order to ascertain the validity of this approach, we carried out one geometry optimization using fully relativistic pseudopotentials. Then, the NMR parameters were calculated using scalar-relativistic PPs. The functional used was PBE. The results (Table S13) show that the use of the scalar-relativistic approximation for the geometry optimization is justified as the errors are below our best MAEs. It is however still possible that spin orbit coupling effects may have a sizable contribution to the NMR parameters and our MAEs may be further reduced using this approach in future studies.

Table S13: results of scalar-relativistic vs fully relativistic calculations on Cs_2CrO_4.

	Unit cell volume [Å^3]			Optimization wall time on 32 cores [d]		|Cq| [kHz]			δ_{iso} [ppm]		
	exp	Scalar relativistic	Fully relativistic	Scalar relativistic	Fully relativistic	exp	Scalar relativistic	Fully relativistic	exp	Scalar relativistic	Fully relativistic
site I	594.61	630.10	634.70	3.5	8.5	365[16] 376[17] 373[18]	390.8	388.6	-98.3[18] -100[17]	-69.4	-64.2
site II						142[16] 138[17] 142[18]	-136.1	-130.1	28.7[18] 28.2[16] 27.0[17]	26.8	27.4

Comparison with fully relativistic chemical shift calculations

Very few examples of fully relativistic ^{133}Cs chemical shift DFT calculations are available in the literature. One of them[33] does not include any comparison with experimental data, preventing an assessment of the importance of SOC incorporation. The other[32] provides both the experimental chemical shift values and fully-relativistic computational results, allowing such an assessment.

The calculations in ref [32] were carried out by fully-relativistic PBE+D3 optimization, followed by the generation of local clusters of a central cation surrounded by a PbI_3 cage representing the asymmetric unit of the periodic crystal structure, which was used for a fully relativistic BP86+D3 calculation of chemical shielding. Our methods therefore differ from those not only by the inclusion of SOC but also by the use of the cluster method and of the BP86 functional, which were not tested here. The results (Figure S6) show that the fully relativistic calculation sometimes outperforms the scalar-relativistic one to an extent which is highly system-dependent. This phenomenon is mediated not only by Cs but obviously also by Pb. In the absence of other systems for which both experimental ^{133}Cs chemical shift values and fully-relativistic computational ones are available, it is hard to draw any further conclusions.

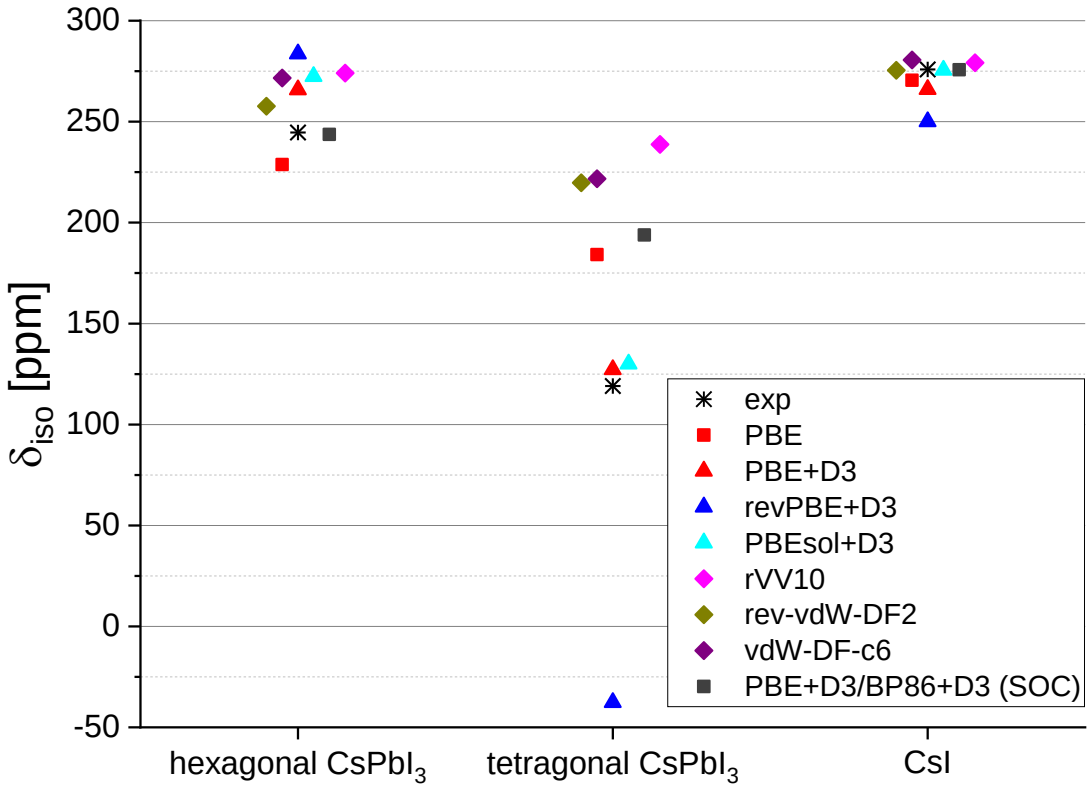

Figure S6: Comparison of chemical shift values calculated with and without SOC. The values with SOC, as well as the experimental values, are taken from[32].

References

(1) Davey, W. P. Precision Measurements of Crystals of the Alkali Halides. *Phys. Rev.* **1923**, *21* (2), 143.
(2) Wyckoff, R. W. *Crystal Structures*, 2nd ed.; Interscience: New York, 1963; Vol. 5.
(3) Morris, A.; Kennard, C.; Moore, F.; Smith, G.; Berendsen, H. J. C. Cesium Chromate, CrCs2O4 (Neutron). *Cryst. Struct. Commun.* **1981**, *10* (3), 529–532.
(4) Granzin, J. Refinement of the Crystal Structures of RbClO4 and CsClO4. *Z. Für Krist.-Cryst. Mater.* **1988**, *184* (1–4), 157–160.
(5) Weber, H.; Schulz, M.; Schmitz, S.; Granzin, J.; Siegert, H. Determination and Structural Application of Anisotropic Bond Polarisabilities in Complex Crystals. *J. Phys. Condens. Matter* **1989**, *1* (44), 8543.
(6) Hawthorne, F.; Calvo, C. The Crystal Chemistry of the M+ VO3 (M+= Li, Na, K, NH4, Tl, Rb, and Cs) Pyroxenes. *J. Solid State Chem.* **1977**, *22* (2), 157–170.
(7) Hooper, R. W.; Ni, C.; Tkachuk, D. G.; He, Y.; Terskikh, V. V.; Veinot, J. G.; Michaelis, V. K. Exploring Structural Nuances in Germanium Halide Perovskites Using Solid-State 73Ge and 133Cs NMR Spectroscopy. *J. Phys. Chem. Lett.* **2022**, *13* (7), 1687–1696.
(8) Thiele, G.; Messer, D. S-Thiocyanato-und N-Isothiocyanato-Bindungsisomerie in Den Kristallstrukturen von RbCd (SCN) 3 Und CsCd (SCN) 3. *Z. Für Anorg. Allg. Chem.* **1980**, *464* (1), 255–267.
(9) Behrens, U.; Hoffmann, F.; Olbrich, F. Solid-State Structures of Base-Free Lithium and Sodium Tetraphenylborates at Room and Low Temperature: Comparison with the Higher Homologues MB (C6H5) 4 (M= K, Rb, Cs). *Organometallics* **2012**, *31* (3), 905–913.
(10) Moon, C. J.; Park, J.; Im, H.; Ryu, H.; Choi, M. Y.; Kim, T. H.; Kim, J. Chemical Shift and Second-Order Quadrupolar Effects in the Solid-State 133Cs NMR Spectra of [Cs+ (Cryptand [2.2. 2])] X (X= I−, SCN−· H2O). *Bull. Korean Chem. Soc.* **2020**, *41* (7), 702–708.
(11) Kaneko, S.; Tokuda, Y.; Takahashi, Y.; Masai, H.; Ueda, Y. Structural Analysis of Mixed Alkali Borosilicate Glasses Containing Cs+ and Na+ Using Strong Magnetic Field Magic Angle Spinning Nuclear Magnetic Resonance. *J. Asian Ceram. Soc.* **2017**, *5* (1), 7–12.
(12) Rakhmatullin, A.; Allix, M.; Polovov, I. B.; Maltsev, D.; Chukin, A. V.; Bakirov, R.; Bessada, C. Combining Solid State NMR, Powder X-Ray Diffraction, and DFT Calculations for CsSc3F10 Structure Determination. *J. Alloys Compd.* **2019**, *787*, 1349–1355.
(13) Ying, Y.; Luo, X.; Huang, H. Pressure-Induced Topological Nontrivial Phase and Tunable Optical Properties in All-Inorganic Halide Perovskites. *J. Phys. Chem. C* **2018**, *122* (31), 17718–17725.
(14) Trots, D.; Myagkota, S. High-Temperature Structural Evolution of Caesium and Rubidium Triiodoplumbates. *J. Phys. Chem. Solids* **2008**, *69* (10), 2520–2526.
(15) Fadla, M. A.; Bentria, B.; Dahame, T.; Benghia, A. First-Principles Investigation on the Stability and Material Properties of All-Inorganic Cesium Lead Iodide Perovskites CsPbI3 Polymorphs. *Phys. B Condens. Matter* **2020**, *585*, 412118.
(16) Skibsted, J.; Vosegaard, T.; Bildsøe, H.; Jakobsen, H. J. 133Cs Chemical Shielding Anisotropies and Quadrupole Couplings from Magic-Angle Spinning NMR of Cesium Salts. *J. Phys. Chem.* **1996**, *100* (36), 14872–14881.
(17) Power, W. P.; Mooibroek, S.; Wasylishen, R. E.; Cameron, T. S. Cesium-133 Single-Crystal NMR Study of Cesium Chromate. *J. Phys. Chem.* **1994**, *98* (6), 1552–1560.
(18) Power, W. P.; Wasylishen, R. E.; Mooibroek, S.; Pettitt, B. A.; Danchura, W. Simulation of NMR Powder Line Shapes of Quadrupolar Nuclei with Half-Integer Spin at Low-Symmetry Sites. *J. Phys. Chem.* **1990**, *94* (2), 591–598.
(19) Kroeker, S.; Schuller, S.; Wren, J. E.; Greer, B. J.; Mesbah, A. 133 Cs and 23 Na MAS NMR Spectroscopy of Molybdate Crystallization in Model Nuclear Glasses. *J. Am. Ceram. Soc.* **2016**, *99* (5), 1557–1564.
(20) Wu, G.; Terskikh, V. A Multinuclear Solid-State NMR Study of Alkali Metal Ions in Tetraphenylborate Salts, M [BPh4](M= Na, K, Rb and Cs): What Is the NMR Signature of Cation− π Interactions? *J. Phys. Chem. A* **2008**, *112* (41), 10359–10364.
(21) Aguiar, P. M. Multinuclear Magnetic Resonance Investigations of Structure and Order in Borates and Metal Cyanides. **2007**.
(22) Czernek, J.; Brus, J. Describing the Anisotropic 133Cs Solid State NMR Interactions in Cesium Chromate. *Chem. Phys. Lett.* **2017**, *684*, 8–13.
(23) Perras, F. A.; Bryce, D. L. Multinuclear Magnetic Resonance Crystallographic Structure Refinement and Cross-Validation Using Experimental and Computed Electric Field Gradients: Application to Na2Al2B2O7. *J. Phys. Chem. C* **2012**, *116* (36), 19472–19482.
(24) Stone, N. Table of Nuclear Electric Quadrupole Moments. *At. Data Nucl. Data Tables* **2016**, *111*, 1–28.
(25) Cheng, J. T.; Edwards, J. C.; Ellis, P. D. Measurement of Quadrupolar Coupling Constants, Shielding Tensor Elements and the Relative Orientation of Quadrupolar and Shielding Tensor Principal Axis

Systems for Rubidium-87 and Rubidium-85 Nuclei in Rubidium Salts by Solid-State NMR. *J. Phys. Chem.* **1990**, *94* (2), 553–561.
(26) Vosegaard, T.; Skibsted, J.; Bildsøe, H.; Jakobsen, H. J. Quadrupole Coupling and Anisotropic Shielding from Single-Crystal NMR of the Central Transition for Quadrupolar Nuclei. 87Rb NMR of RbClO4and Rb2SO4. *J. Magn. Reson. A* **1996**, *122* (2), 111–119.
(27) Vosegaard, T.; Skibsted, J.; Bildsoe, H.; Jakobsen, H. J. Combined Effect of Second-Order Quadrupole Coupling and Chemical Shielding Anisotropy on the Central Transition in MAS NMR of Quadrupolar Nuclei. 87Rb MAS NMR of RbClO4. *J. Phys. Chem.* **1995**, *99* (27), 10731–10735.
(28) Hayashi, S.; Hayamizu, K. Accurate Determination of NMR Chemical Shifts in Alkali Halides and Their Correlation with Structural Factors. *Bull. Chem. Soc. Jpn.* **1990**, *63* (3), 913–919.
(29) Haase, A.; Kerber, M.; Kessler, D.; Kronenbitter, J.; Krüger, H.; Lutz, O.; Müller, M.; Nolle, A. Nuclear Magnetic Shielding and Quadrupole Coupling of 133Cs in Cesium Salt Powders. *Z. Für Naturforschung A* **1977**, *32* (9), 952–956.
(30) Mooibroek, S.; Wasylishen, R. E.; Dickson, R.; Facey, G.; Pettitt, B. A. Simultaneous Observation of Shielding Anisotropies and Quadrupolar Splittings in Solid State 133Cs NMR Spectra. *J. Magn. Reson. 1969* **1986**, *66* (3), 542–545.
(31) Wong, A.; Sham, S.; Wang, S.; Wu, G. A Solid-State 133Cs Nuclear Magnetic Resonance and X-Ray Crystallographic Study of Cesium Complexes with Macrocyclic Ligands. *Can. J. Chem.* **2000**, *78* (7), 975–985.
(32) Kubicki, D. J.; Prochowicz, D.; Hofstetter, A.; Zakeeruddin, S. M.; Grätzel, M.; Emsley, L. Phase Segregation in Cs-, Rb-and K-Doped Mixed-Cation (MA) x (FA) 1–x PbI3 Hybrid Perovskites from Solid-State NMR. *J. Am. Chem. Soc.* **2017**, *139* (40), 14173–14180.
(33) Haq, I. U.; Ali, A.; Khan, I. Investigation of NMR Shielding, EFG and Structural Relaxation of All-Inorganic Pb-Based Ruddlesden Popper Halide Perovskites. *Appl. Phys. A* **2023**, *129* (12), 875.